

# Evolution with Magnetic Field of Discrete Scale Invariant Supercritical States in Graphene

Hailong Li,<sup>1</sup> Haiwen Liu,<sup>2</sup> Robert Joynt,<sup>3,4,\*</sup> and X. C. Xie<sup>1,5,6,†</sup>

<sup>1</sup>*International Center for Quantum Materials, School of Physics, Peking University, Beijing 100871*

<sup>2</sup>*Center for Advanced Quantum Studies, Department of Physics, Beijing Normal University, Beijing 100875*

<sup>3</sup>*Kavli Institute of Theoretical Sciences, Chinese Academy of Sciences, Beijing 100049*

<sup>4</sup>*Department of Physics, University of Wisconsin-Madison, 1150 Univ. Ave., Madison WI 53706 USA*

<sup>5</sup>*Beijing Academy of Quantum Information Sciences, Beijing 100193, China*

<sup>6</sup>*CAS Center for Excellence in Topological Quantum Computation, University of Chinese Academy of Sciences, Beijing 100190, China*

(Dated: January 7, 2022)

We investigate the quasi-bound states of a Coulomb impurity in graphene in the presence of a magnetic field. These states exhibit the dramatic and rather rare property of discrete scale invariance when the Coulomb potential is supercritical. We show using both Wentzel-Kramers-Brillouin (WKB) approximation and numerical studies that the supercritical states are converted to subcritical states as the field is increased. The local density of states is calculated and it shows direct signatures of discrete scale invariance. In a magnetic field, these signatures are gradually destroyed in a systematic way. Hence the effect that we propose can be detected via scanning tunneling microscope experiments. The range of magnetic field and energy resolution required are compatible with existing experimental setups. These experiments can be performed in a single sample by changing the field; they do not involve changing the nuclear charge.

## I. INTRODUCTION

Since the successful isolation of graphene in 2007 [1], it has been an ideal two-dimensional system to realize ultra-relativistic phenomena and quantum electrodynamics [2–4]. One of the most striking and novel effects is the collapse of an atomic wavefunction when the nuclear charge parameter  $Z$  exceeds a critical value  $Z_c$  [5]. This was predicted many years ago for atoms in free space [6–8]. Unfortunately, the expected  $Z_c \sim 170$  made it difficult to observe this phenomenon [6, 9]. However, quasiparticles in graphene are two-dimensional massless Dirac fermions and their velocity is  $v_F \approx 10^6 m/s$ , which is two orders of magnitude smaller than the speed of light [10, 11]. Thus the effective fine structure constant in graphene becomes  $\alpha = Ze^2/\kappa\hbar v_F \sim \mathcal{O}(1) \gg \alpha_0 \approx 1/137$ , where  $\alpha_0$  is the bare fine-structure constant. So graphene provides a promising platform to investigate the supercritical atomic collapse phenomenon. For this reason, Coulomb scattering and atomic collapse in graphene have aroused a great deal of interest [12–20]. Due to Klein tunneling and zero mass in graphene, there are no true bound states. For the subcritical case  $\alpha < |m|$ , there are not even sharp resonances [16]. By contrast, in the supercritical regime with  $\alpha > |m|$ , an infinite series of quasi-bound states exist, and these states show a dramatic property: discrete scale invariance (DSI), reminiscent of the Efimov trimer states [19, 21–24]. In particular, the resonances associated with this atomic collapse were observed successfully in scanning tunneling microscope (STM) experiments [18, 25–27].

DSI has also been observed in bulk three-dimensional materials by the detection of a new type of quantum oscillation in the magneto-resistance  $R(B)$  [28].  $R(B)$  is periodic in  $\ln(B)$  in certain topological Dirac materials under ultrahigh magnetic fields. This arises from the Coulomb impurity quasi-bound states in the material [24].

In graphene, samples are usually intercalation compounds of graphene [29] or sheets with charged vacancies [30]. In the graphene experiments cited above it is necessary to prepare different samples with different values of  $\alpha$  to test the existence of these quasi-bound states [31]. Here, we propose that even in a single sample with a given supercritical  $\alpha$ , the magnetic field can induce qualitative changes in the quasi-bound states. This leads to an observable transition from the supercritical regime to the subcritical one. One can understand the basic idea using a semiclassical argument: the application of  $\mathbf{B}$  in the  $z$ -direction produces a flux through the electronic wavefunction, and consequently the angular momentum number  $m$  will be modified into an effective quantum number  $m_{eff}$ . This means that a quasi-bound state in the presence of a potential with a fixed effective  $\alpha$  will lead to a transition from supercritical (DSI) regime to the subcritical (non-DSI) regime when  $B$  is increased.  $B$  provides a long-distance cutoff at a distance  $l_B = \sqrt{\hbar c/eB}$  and converts supercritical states with effective radius longer than  $l_B$  into subcritical states. Some states should undergo this conversion when  $B$  is in the range of a few Tesla.

In the Sec. II, we give analytical results to support the basic argument. In Sec. III we present detailed numerical calculations that can be compared with experiments. Sec. IV is a short summary.

\* rjoynt@wisc.edu

† xcxie@pku.edu.cn

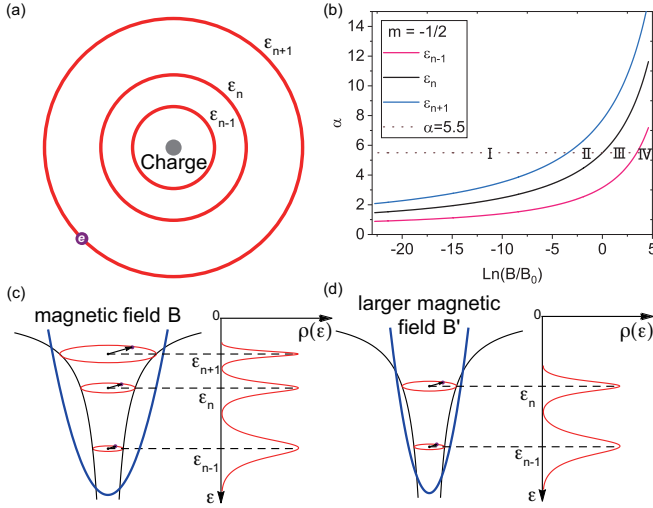


FIG. 1. (color online) (a) Semiclassical picture of the orbits of the supercritical states with energies,  $\epsilon_{n+1}$ ,  $\epsilon_n$  and  $\epsilon_{n-1}$ , with  $m = -1/2$ ,  $\alpha = 5.5$  and zero magnetic field. The radii exhibit the discrete scale invariance of these states. (b) The transitions of the three states from supercritical to subcritical.  $B_0$  is related to the short range cut-off  $r_a$  with  $\sqrt{\hbar c/eB_0} = r_a$ . It shows the critical  $\alpha$  approaches the limit  $1/2$  as the magnetic field  $B$  goes to 0. Moreover, the points of intersection of the dash-dotted line and the three solid curves give us the critical magnetic field which converts the supercritical state into a subcritical one with  $\alpha = 5.5$ . (c) and (d) A schematic picture of the process by which a supercritical state is converted to a subcritical one as  $B$  increases.

## II. THEORETICAL MODEL

In this section we review the  $B = 0$  case that can be solved exactly and show that a kind of Wentzel-Kramers-Brillouin (WKB) approximation gives good results for finite  $B$  in the regime of interest. The 2D massless Dirac equation with a Coulomb potential is

$$\frac{1}{\hbar} \left( \boldsymbol{\sigma} \cdot (\mathbf{p} + e\mathbf{A}/c) - \frac{\alpha}{r} \right) \psi(\mathbf{r}) = \varepsilon \psi(\mathbf{r}), \quad (1)$$

where  $\psi(\mathbf{r})$  is a two-component wave function,  $\boldsymbol{\sigma}$  denotes the Pauli matrices, and  $\varepsilon = E/\hbar v_F$ , where  $E$  is the energy. We adopt the symmetric gauge for the magnetic vector potential,  $\mathbf{A} = (-By/2, Bx/2, 0)$ . In addition we impose a short distance cutoff at  $r = r_a$  where  $r$  is the radial coordinate such that the potential  $V(\mathbf{r}) = Ze^2/\kappa\hbar c r_a$  for  $r < r_a$ . The region  $r_a \ll r \ll l_B$  is the scale-invariant region: when  $r$  is in this range, all operators have dimension  $(\text{length})^{-1}$ .

We firstly review the analytic solution to the  $B = 0$  case. By introducing cylindrical coordinates, we can separate the equation and obtain a general solution in the following form:

$$\psi(r, \phi) = \frac{u_2}{\sqrt{r}} \begin{pmatrix} 1 \\ 0 \end{pmatrix} e^{i(m-1/2)\phi} + i \frac{u_1}{\sqrt{r}} \begin{pmatrix} 0 \\ 1 \end{pmatrix} e^{i(m+1/2)\phi} \quad (2)$$

where  $m$  is a half-integer angular momentum quantum number,  $u_1(r)$  and  $u_2(r)$  are the radial functions. For  $\alpha < |m|$  or subcritical case, the solutions do not yield any quasi-bound states, and the only non-trivial effect is the so-called Coulomb phase shift [32]. When  $\alpha > |m|$ , the supercritical case, a cut-off for the Coulomb potential at a small  $r_a$  is necessary for avoiding a divergence [33, 34]. We choose a soft cutoff such that  $V(r) = Ze^2/\kappa r_a$  for  $r \leq r_a$ . The results are not sensitive to the details of the cutoff. The states are sharp resonances with quasi-energies [18]

$$\frac{\varepsilon_{n+1}}{\varepsilon_n} \propto e^{-\pi/\sqrt{\alpha^2 - m^2}}, \quad (3)$$

where  $n$  is the radial (principal) quantum number. The quasi-energies forms a geometric series. We give a schematic picture of the states in Fig. 1a.

For  $B > 0$  one can apply the WKB approximation to Eq. (1) to describe the supercritical quasi-bound states when  $\alpha$  exceeds a certain value that now depends on  $B$ . This method will also allow us to understand how the external magnetic field can be thought of as an effective angular momentum,  $m_{eff}$ , replacing the angular momentum  $m$  of the  $B = 0$  case. The appropriate radial momentum is

$$p_r^2 = \left( \frac{E}{\hbar v_F} + \frac{\alpha}{r} \right)^2 - \left( \frac{m}{r} - \frac{r}{2l_B^2} \right)^2. \quad (4)$$

The Bohr-Sommerfeld quantization condition is  $\int_{r_0}^{r_1} p_r dr = n\pi\hbar$ , where  $r_0$  and  $r_1$  are turning points of Eq. (4). The quasi-bound states form in the classically permitted region and they can tunnel to the outer region via Klein tunneling. With the WKB method, scattering coefficients can be obtained analytically and the numerical results of the local density of states are shown in Fig. 2.

The condition for the transition from supercritical to subcritical can be written in an intuitive form as follows. For the  $n$ th state, we rewrite  $r/(2l_B^2)$  as  $\mathbf{B} \cdot \mathbf{S}_n / (2\Phi_0 r)$ , where  $S_n$  is the rms area of the part of the wavefunction of the  $n$ th supercritical state that lies inside the potential barrier.  $\Phi_0 = h/(2e)$  denotes the magnetic flux quantum. So, it is natural to define  $\mathbf{B} \cdot \mathbf{S}_n / (2\Phi_0)$  as a new physical quantity,  $N_{B,n}$ , which is one half the number of magnetic flux quanta enclosed by the  $n$ th supercritical state in the scale-invariant region. Then, we also define the absolute value of the effective angular momentum quantum number as  $|m_{eff}| = |m - N_{B,n}|$ . Thus the Bohr-Sommerfeld condition gives a relation  $\alpha(B)$  that is plotted in Fig. 1b. As  $B$  increases, the  $n$ th state makes a transition from supercritical to subcritical when  $\alpha = |m_{eff}|$ . Taking the physical value of  $\alpha$ , we get a critical value  $B_n$  for which there is a sudden transition from a very narrow resonance to an extremely broad one. We show this for three states and  $\alpha = 5.5$ . As we shall see, their identifiable contribution to the LDOS effectively disappears as they successively pass through the transition. In Fig 1c

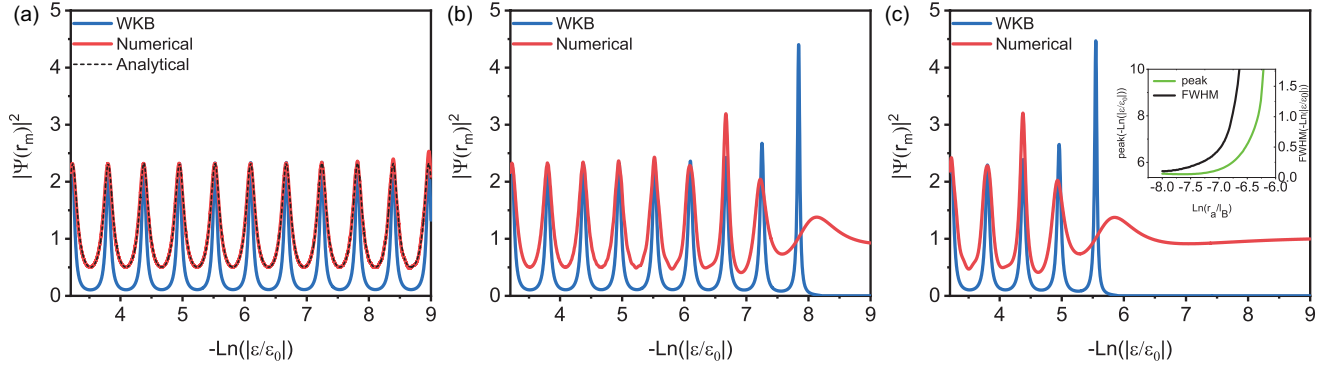


FIG. 2. (color online) LDOS for the angular momentum channel  $m = -1/2$  at a given radius  $r_m$ . Here  $\alpha = 5.5$ , the dimensionless energy is plotted on a log scale and  $\epsilon_0$  is related to the fermi energy. The pink solid line, blue solid line and the black dashed line denote the results given by the numerical method, WKB method and analytical method respectively. As  $B$  increases, the supercritical states with smaller binding energies are converted to the subcritical ones earlier than the larger ones. The inset in (c) shows the peak broadening and the binding energy decreasing under increasing magnetic field for a given quasi-bound state. The solutions are calculated under three different magnetic fields: (a)  $l_B = 10^6 r_a$ ; (b)  $l_B = 5 \times 10^4 r_a$ ; (c)  $l_B = 5 \times 10^3 r_a$ . Here,  $r_a$  is a cut-off for the Coulomb potential.

all three states are supercritical; Fig. 1d corresponds to the case where the  $n - 1$  and  $n$  state are still visible but the  $n + 1$  state is not.

### III. NUMERICAL APPROACH

The 2D massless Dirac equation with  $B > 0$  can be solved numerically. This is necessary since the WKB approximation is always poor near the turning points. However, the numerics will show that WKB is still reliable as a semi-quantitative guide.

We start from the radial equation, Eq. (5), and use the finite difference method. The radial equation can be derived by substituting Eq. (2) into Eq. (1), which gives

$$\frac{d}{dr} \begin{bmatrix} u_1(r) \\ u_2(r) \end{bmatrix} = \begin{bmatrix} -\frac{m}{r} + \frac{r}{2l_B^2} & \frac{E}{\hbar v_F} - V(r) \\ -\frac{E}{\hbar v_F} + V(r) & \frac{m}{r} - \frac{r}{2l_B^2} \end{bmatrix} \begin{bmatrix} u_1(r) \\ u_2(r) \end{bmatrix}. \quad (5)$$

In Eq. (5),  $V(r)$  is the modified Coulomb potential with the above-mentioned soft cutoff at  $r_a$ . Eliminating  $u_2$  gives the final approximate radial equation for  $u_1$  as:

$$u_1''(r) = \left[ \left( \frac{m}{r} - \frac{r}{2l_B^2} \right)^2 - \left( \frac{E}{\hbar v_F} - V(r) \right)^2 \right] u_1(r), \quad (6)$$

after which  $u_2$  is easily solved.

The following discussion is based on numerical solutions of these equations.

#### A. Validation of Numerics

The LDOS for the lowest angular momentum channel  $m = -1/2$  obtained by three different methods is shown in Fig. 2, enabling the reader to compare the different

methods. In Fig. 2, we set  $\alpha = 5.5$ , and plot the LDOS at an arbitrarily given location  $r_m$  in logarithmic scale. In Fig. 2a, the magnetic field is so weak that it almost does not affect the effective angular momentum of the quasi-bound states and they all remain supercritical. The results given by analytical solution and numerical method fit each other very well, and the results of WKB approximation shows similar peak values but slightly different widths. In the log-scale energy plot shown in Fig. 2, peak values behave as an arithmetic sequence, which reveals the DSI of these quasi-bound states. For larger  $B$ , the analytic method is inapplicable, so only the WKB and finite-difference results are plotted in Fig. 2b,c. As  $B$  increases, the quasi-bound states begin to “disappear” – their width increases so rapidly that they leave no signature in the LDOS. As an illustration, the inset in Fig. 2c shows that the binding energy of a given quasi-bound state decreases and the corresponding full width half maximum (FWHM) becomes wider with the increasing magnetic field. The numerical results agree well with the WKB results, except for the state with smallest binding energy, of which the energy peak shows a minor difference. However, the transition fields for the “disappearance” of the quasi-bound state are nearly the same with the two methods. These results confirm the argument of the previous section that these transitions occur when  $|m_{eff}| = \alpha$ .

#### B. Local Density of States in STM Experiments

We calculate the LDOS as a function of energy and distance away from the charged impurity by the numerical method for a few representative values of  $B$ , with the results shown in Fig. 3. The three subgraphs are all plotted on log scale. Larger numbers in the vertical axis refer to smaller binding energies, while smaller numbers

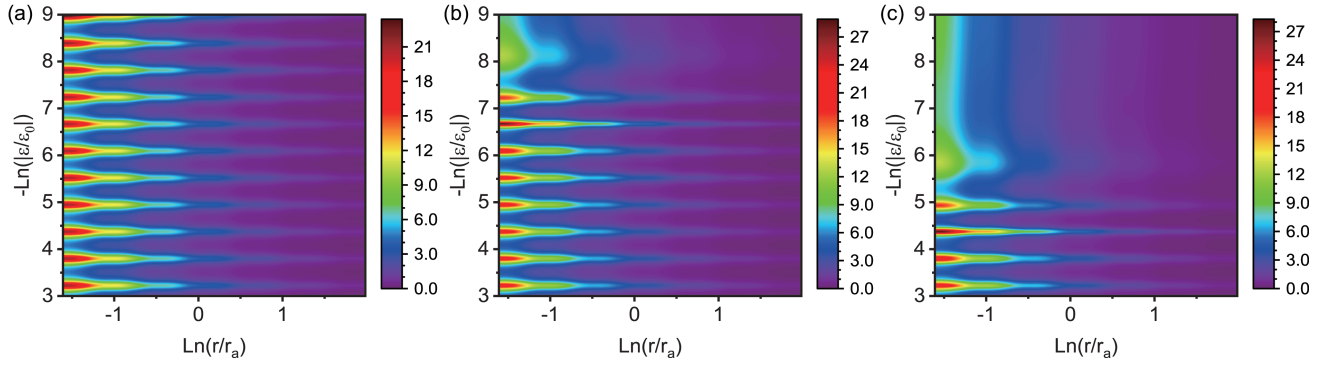


FIG. 3. (color online) Local density of states for the angular momentum channel  $m = -1/2$  and potential strength  $\alpha = 5.5$ . The LDOS is plotted as a function of energy and distance away from the charged impurity for three different magnetic fields on a log scale. Both discrete scale invariance and the transitions from supercritical to subcritical are directly reflected in the LDOS. (a)  $l_B = 10^6 r_a$ ; (b)  $l_B = 5 \times 10^4 r_a$ ; (c)  $l_B = 5 \times 10^3 r_a$ .

refer to larger binding energies. Fig. 3a shows a series of supercritical states for small  $B$ . The typical periodicity in  $\ln \epsilon$  is evident. The overall physical picture is strikingly confirmed by the appearance of one broad resonance between the series of narrow resonances and the continuum at small energies. The larger magnetic field in Fig. 3b converts some supercritical states with smaller binding energies into subcritical ones with the rest of the quasi-bound states still satisfying discrete scale invariance. More supercritical states disappear due to a much larger magnetic field in Fig. 3c. Therefore, with increasing magnetic field, the supercritical states are converted to subcritical ones and disappear from small binding energies to large binding energies. Although the external magnetic field affects the existence of some quasi-bound states, it does not destroy the distribution of the rest of the supercritical states and the property of discrete scale invariance.

The results in Fig. 3 can be directly checked in STM experiments under a magnetic field. For example, if we draw a vertical line at a given radius  $r_m$  in Fig. 3 the oscillations will be visible as the voltage is varied. When the experiment is repeated at larger  $B$ , the oscillations in the LDOS will disappear one by one.

### C. Multiple Angular Momentum Channels

In the previous section we focused on a single angular momentum channel, which produced a relatively simple picture of the LDOS. When multiple channels are present, the situation is more complicated. We first note that this physical system has time-reversal symmetry when  $B = 0$ , which guarantees the degeneracy between  $m$  and  $-m$  channels. These degenerate quasi-bound states separately satisfy DSI. The non-zero magnetic field will break the degeneracy, but DSI can not be hidden if there is a near degeneracy.

For further comparison, we calculate the LDOS for the case of  $m = 1/2$ , the counterpart of  $m = -1/2$ . In Fig. 4c

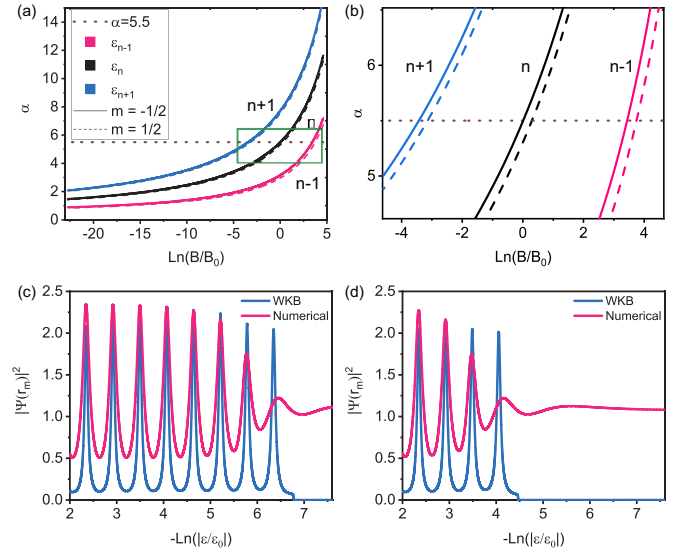


FIG. 4. (color online) (a) The critical  $\alpha$  as a function of the magnetic field. It shows the critical  $\alpha$  approaches the limit  $1/2$  as the magnetic field  $B$  goes to 0. Here,  $B_0$  is defined as  $\sqrt{\hbar/(eB_0)} = r_a$ . For  $\alpha = 5.5$ ,  $\Delta \text{Log}(B/B_0)$  between  $\epsilon_{n+1}$  and  $\epsilon_n$  is  $-3.44$  as well as  $-3.43$  between  $\epsilon_n$  and  $\epsilon_{n-1}$  when  $m = -1/2$ . As for  $m = 1/2$ ,  $\Delta \text{Log}(B/B_0)$  between  $\epsilon_{n+1}$  and  $\epsilon_n$  is  $-3.44$ , while the one between  $\epsilon_n$  and  $\epsilon_{n-1}$  is  $-3.45$ . It proves that the degeneracy breaking by the magnetic field won't affect the observation of the supercritical states and the process in which the supercritical states converts to the subcritical states especially for large  $\alpha$ . (b) the zoom-in plot of the green rectangle in Fig. 4a. (c) LDOS obtained by numerical method and WKB method with the magnetic length  $l_B = 5 \times 10^4 r_a$  and  $m = 1/2$ . (d) LDOS obtained by numerical method and WKB method with the magnetic length  $l_B = 5 \times 10^3 r_a$  and  $m = 1/2$ .

and 4d, we compare the different solutions calculated by the numerical method and WKB method with different magnetic fields as we did in Fig. 2. It behaves the same as in the case of  $m = -1/2$ . The log-scale energy levels



behave as an arithmetic sequence and the log-scale energy difference is nearly the same as that of  $m = -1/2$ , and the presence of DSI is clear. Once again, as  $B$  increases, the supercritical states with smaller binding energies are converted to the subcritical states earlier than the larger ones.

For an arbitrary magnetic field, we use the Bohr-Sommerfeld quantization condition as in Fig. 1b to calculate the critical  $\alpha$  as a function of the magnetic field for given supercritical states. Here, we only consider the case when the Landau level spacing is smaller than the Coulomb attraction energy. The comparison of  $m = -1/2$  and  $m = 1/2$  is shown in Fig. 4a. Here, the solid lines and the dashed lines represent  $m = -1/2$  and  $m = 1/2$  respectively. The critical  $\alpha$  approaches the limit  $1/2$  as  $B$  goes to 0. As we have discussed in Sect. I, these critical magnetic fields also satisfy DSI for both cases. As shown in Fig. 4b, with enlarging the magnetic field along the horizontal dash-dotted line, the  $n$ -th supercritical state becomes subcritical when crossing the line labelled by  $n$ .

We have focused on the lowest angular momentum channels, since the higher ones are less likely to show up in experiments. The degeneracy breaking resulting from the external magnetic field does not cause significant differences between  $m$  and  $-m$ , especially for large  $\alpha$ . Guaranteed by these aforementioned conditions, the evolution process of the supercritical states can be observed in experiments by STM. From previous experiments [28], the value  $\alpha = 5.5$  seems the most reasonable. Assuming a cutoff  $r_a = 0.5nm$ , we can estimate that in the range from  $B = 10^{-2}T$  to  $B = 2T$ , three or four

quasi-bound states will disappear. This is a convenient range for many experiments. Their energies are in the range of 10 meV, so very high energy resolution is not required.

#### IV. SUMMARY

We have investigated the LDOS of quasi-bound states in graphene with a supercritical Coulomb potential. These supercritical states exhibit a dramatic property: discrete scale invariance. We propose that the external magnetic field can change the effective angular momentum for each definite supercritical state and convert it to a subcritical one. We show the local density of states for a given angular momentum channel, an observable quantity, reveals directly that these supercritical states vanish one by one starting from small binding energies and proceeding to large binding energies as the field increases. Moreover, the critical magnetic field values also satisfies the property of discrete scale invariance. Our proposal can be verified by LDOS measurement in STM experiments.

#### Acknowledgements

We thank Ziqiang Wang and Qing-Feng Sun for valuable discussions. This work was financially supported by the National Basic Research Program of China (Grants No. 2017YFA0303301, No. 2015CB921102), the National Natural Science Foundation of China (Grants No. 11674028, No. 11534001, No. 11504008), and the Fundamental Research Funds for the Central Universities.

- 
- [1] A. K. Geim and K. S. Novoselov, Nat. Mater. **6**, 183 (2007).
  - [2] M. I. Katsnelson and K. S. Novoselov, Solid State Commun. **143**, 3 (2007).
  - [3] M. I. Katsnelson, K. S. Novoselov, and A. K. Geim, Nat. Phys. **2**, 620 (2006).
  - [4] J. González, F. Guinea, and M. A. H. Vozmediano, Nucl. Phys. B **424**, 595 (1994).
  - [5] T. H. Boyer, Am. J. Phys. **72**, 992 (2004).
  - [6] W. Greiner, B. Müller, and J. Rafelski, *Quantum electrodynamics of strong fields: with an introduction into modern relativistic quantum mechanics* (Springer, 1985).
  - [7] Y. B. Zeldovich and V. S. Popov, Sov. Phys. Usp. **14**, 673 (1972).
  - [8] I. Pomeranchuk and Y. Smorodinsky, J. Phys. USSR **9**, 97 (1945).
  - [9] V. S. Popov, Phys. At. Nucl. **64**, 367 (2001).
  - [10] A. H. Castro Neto, F. Guinea, N. M. R. Peres, K. S. Novoselov, and A. K. Geim, Rev. Mod. Phys. **81**, 109 (2009).
  - [11] E. Y. Andrei, G. Li, and X. Du, Rep. Prog. Phys. **75**, 056501 (2012).
  - [12] K. Nomura and A. H. MacDonald, Phys. Rev. Lett. **96**, 256602 (2006).
  - [13] E. H. Hwang, S. Adam, and S. Das Sarma, Phys. Rev. Lett. **98**, 186806 (2007).
  - [14] D. S. Novikov, Phys. Rev. B **76**, 245435 (2007).
  - [15] V. M. Pereira, J. Nilsson, and A. H. Castro Neto, Phys. Rev. Lett. **99**, 166802 (2007).
  - [16] A. V. Shytov, M. I. Katsnelson, and L. S. Levitov, Phys. Rev. Lett. **99**, 246802 (2007).
  - [17] V. M. Pereira, V. N. Kotov, and A. H. Castro Neto, Phys. Rev. B **78**, 085101 (2008).
  - [18] A. V. Shytov, M. I. Katsnelson, and L. S. Levitov, Phys. Rev. Lett. **99**, 236801 (2007).
  - [19] Y. Nishida, Phys. Rev. B **90**, 165414 (2014).
  - [20] Y. Nishida, Phys. Rev. B **94**, 085430 (2016).
  - [21] V. Efimov, Phys. Lett. B **33**, 563 (1970).
  - [22] D. Sornette, Phys. Rep. **297**, 239 (1998).
  - [23] V. N. Efimov, Sov. J. Nucl. Phys. **12**, 589 (1971).
  - [24] H. Liu, H. Jiang, Z. Wang, R. Joynt, and X. C. Xie, arXiv e-prints, arXiv:1807.02459 (2018), arXiv:1807.02459 [cond-mat.mtrl-sci].
  - [25] P. M. Ostrovsky, I. V. Gornyi, and A. D. Mirlin, Phys. Rev. B **74**, 235443 (2006).
  - [26] O. Ovdut, J. Mao, Y. Jiang, E. Y. Andrei, and E. Akkermans, Nat. Commun. **8**, 507 (2017).
  - [27] Y. Wang, D. Wong, A. V. Shytov, V. W. Brar, S. Choi,

- Q. Wu, H.-Z. Tsai, W. Regan, A. Zettl, R. K. Kawakami, S. G. Louie, L. S. Levitov, and M. F. Crommie, *Science* **340**, 734 (2013).
- [28] H. Wang, H. Liu, Y. Li, Y. Liu, J. Wang, J. Liu, J.-Y. Dai, Y. Wang, L. Li, J. Yan, D. Mandrus, X. C. Xie, and J. Wang, *Sci. Adv.* **4**, eaau5096 (2018).
- [29] M. S. Dresselhaus and G. Dresselhaus, *Adv. Phys.* **51**, 1 (2002).
- [30] J. Mao, Y. Jiang, D. Moldovan, G. Li, K. Watanabe, T. Taniguchi, M. R. Masir, F. M. Peeters, and E. Y. Andrei, *Nat. Phys.* **12**, 545 (2016).
- [31] Y. Wang, V. W. Brar, A. V. Shytov, Q. Wu, W. Regan, H.-Z. Tsai, A. Zettl, L. S. Levitov, and M. F. Crommie, *Nat. Phys.* **8**, 653 (2012).
- [32] L. D. Landau and E. M. Lifshitz, *Quantum mechanics: non-relativistic theory*, Vol. 3 (Elsevier, 2013).
- [33] P. G. Silvestrov and K. B. Efetov, *Phys. Rev. Lett.* **98**, 016802 (2007).
- [34] H.-Y. Chen, V. Apalkov, and T. Chakraborty, *Phys. Rev. Lett.* **98**, 186803 (2007).